Reprinted from *Journal of Dental Research*, Vol. 78, No. 4, 1999

J Dent Res 78(4): 887-897, April, 1999

Damage Modes in Dental Layer Structures

Y.-G. Jung, S. Wuttiphan, I.M. Peterson, and B.R. Lawn*

Materials Science and Engineering Laboratory, National Institute of Standards and Technology, Gaithersburg, Maryland 20899; *to whom correspondence and reprint requests should be addressed

Abstract. Natural teeth (enamel/dentin) and most restorations are essentially layered structures. This study examines the hypothesis that coating thickness and coating/substrate mismatch are key factors in the determination of contact-induced damage in clinically relevant bilayer composites. Accordingly, we study crack patterns in two model "coating/substrate" bilayer systems conceived to simulate crown and tooth structures, at opposite extremes of elastic/plastic mismatch: porcelain on glass-infiltrated alumina ("soft/hard"); and glass-ceramic on resin composite ("hard/soft). Hertzian contacts are used to investigate the evolution of fracture damage in the coating layers, as functions of contact load and coating thickness. The crack patterns differ radically in the two bilayer systems: In the porcelain coatings, cone cracks initiate at the coating top surface; in the glass-ceramic coatings, cone cracks again initiate at the top surface, but additional, upward-extending transverse cracks initiate at the internal coating/substrate interface, with the latter dominant. The substrate is thereby shown to have a profound influence on the damage evolution to ultimate failure in the bilayer systems. However, the cracks are highly stabilized in both systems, with wide ranges between the loads to initiate first cracking and to cause final failure, implying damage-tolerant structures. Finite element modeling is used to evaluate the tensile stresses responsible for the different crack types. The clinical relevance of these observations is considered.

Key words: dental ceramics, fracture, Hertzian contact, layers, teeth.

Received December 23, 1997; Last Revision May 26, 1998; Accepted June 8, 1998

Introduction

Dental structures are essentially layered composites. This is true of both natural teeth (enamel/dentin) and restorations such as crowns, inlays, and bridges (Claus, 1990; Probster and Diehl, 1992; Probster, 1993; Rinke *et al.*, 1995; Wolf, 1995; Giordano, 1996; Hornberger *et al.*, 1996; Wolf *et al.*, 1996; Kelly, 1997). The most aesthetic restorations usually consist of at least one ceramic component, with net outer thickness ranging from 1.5 mm down to 0.5 mm or less near the margins, on a soft dentin interior from 1 to 4 mm thick. Sometimes there is a relatively stiff intervening core, such as alumina, ideally 1 mm thick but again sometimes less. Often there is a thin underlying "bond" layer, *e.g.*, dento-enamel junction (DEJ) in natural teeth or luting cement in crowns, typically tens of μm. As with many other biomechanical systems, the properties of layered structures can be superior to those of their constituent material components.

High masticatory forces may induce fracture or deformation in the dental restoration, either of which can lead to premature failure. Tooth contacts can be closely simulated by indentation with spheres—the so-called Hertzian contact test (Peterson *et al.*, 1998a). In monolithic ceramics, tensile stresses generate macroscopic cone-like cracks around the contact; shear stresses generate diffuse "*quasi*-plastic" damage zones, consisting of distributed grain-localized failures, beneath the contact (Lawn *et al.*, 1994). The dominant damage mode in any given material is dictated by the microstructure: Fine microstructures with minimal internal weakness tend to exhibit macroscopic cracks; coarse microstructures with enhanced internal weakness tend to exhibit *quasi*-plastic zones. Both cracks and *quasi*-plasticity can lead to degradation of properties, and ultimately compromise the useful lifetimes of restorative structures, in different ways (Lawn *et al.*, 1998; Peterson *et al.*, 1998a,b). The two modes may be interactive—plasticity can enhance or inhibit fractures by redistributing tensile stresses.

Recent work has been reported on Hertzian contact stress fields in bilayer structures with a brittle outer layer on either

a hard or soft substrate material. Systems studied include glass/glass-ceramics (Wuttiphan *et al.*, 1996), alumina-based bilayers (An *et al.*, 1996), silicon nitride bilayers (Lee *et al.*, 1998), ceramic/metal systems (Pajares *et al.*, 1996a,b; Wuttiphan *et al.*, 1997), and ceramic/polymer systems (Anusavice and Tsai, 1997). Generally, coating fracture is the dominant source of failure. Such fracture is driven by tensile stresses which concentrate at the surface outside the contact and at the internal interface immediately below the contact, with relative intensities dependent on the interlayer elastic–plastic mismatch (as measured by differences in elastic modulus and hardness) and coating thickness. Debate continues as to which of these two locations of tensile concentration dominates clinical failures of ceramic-based restorations (Kelly, 1997). In systems where the mismatch is small (glass/glass-ceramic bilayers [Wuttiphan *et al.*, 1996]), first crack initiation tends to occur at the top surface; in systems where the mismatch is large and the underlayer is soft (ceramic/metal systems [Pajares *et al.*, 1996a,b; Anusavice and Tsai, 1997]), first initiation tends to occur at the internal interface. Plasticity in the substrate can exacerbate this latter kind of interior fracture. As the load is increased above the cracking threshold, the fracture patterns can become complex, with a multiplicity of co-existent cracks extending both downward from the top surface and upward from the internal interface (and even some initiated within the coating interior) (Lee *et al.*, 1998). Such multiple cracks tend to be highly stable, consistent with the clinical experience of sustainable hairline cracks in tooth enamel, especially in older patients (Kelly, 1997). Such cracks may not always be clearly visible by surface inspection prior to failure.

In this study, we use Hertzian contact (Peterson *et al.*, 1998a) to investigate fracture damage in two model bilayer material systems specifically designed to simulate crown and tooth material structures: porcelain on glass-infiltrated alumina; and glass-ceramic on resin composite. These two systems lie at opposite extremes of elastic/plastic mismatch, and thereby encompass a broad range of coating fracture modes. We use a "bonded-interface" technique to investigate the nature of these crack modes in coatings of different thicknesses (Mulhearn, 1959; Guiberteau *et al.*, 1994; Peterson *et al.*, 1998a). Critical loads for crack initiation are measured. Finite element modeling (Fischer-Cripps and Lawn, 1996b), with parameters "calibrated" from indentation stress-strain curves, is used to analyze the stress states in the bilayers and to rationalize the crack patterns.

Materials and methods

Characterization of component materials

As indicated, the individual material components for our bilayer study were chosen for their clinical relevance, and for their broad spectrum of elastic–plastic properties:

Feldspathic porcelain (Vitadur Alpha, Vita Zahnfabrik, Bad Sackingen, Germany), used as a veneer for crowns and other restorations. In the sintered form, the microstructure consists of a glass matrix containing some undissolved amorphous frit from 1 to 5 μm in scale (confirmed by x-ray analysis). In the present work, the material was used in as-received powder form for sintering onto alumina substrates.

Glass-infiltrated slipcast alumina (InCeram, Vita Zahnfabrik, Bad Sackingen, Germany), used as cores for crowns. The microstructure contains ≈ 80 vol% faceted alumina grains, the largest of which are platelets ≈ 5 μm in diameter and ≈ 1–2 μm thick and the smallest of which are spheres < 0.5 μm, and ≈ 20 vol% lanthanum glass infiltrate (Hornberger *et al.*, 1996). Machined substrate pre-form bars 3 x 4 x 25 mm are glass-infiltrated and sandblasted for removal of excess glass.

Micaceous glass-ceramic (Dicor, Corning Inc., Corning, NY), developed as a crown material for direct fitting onto dentin, with aesthetic properties close to those of dental enamel (Grossman, 1991). The microstructure consists of ≈ 60 vol% mica platelets ≈ 2 μm in diameter and ≈ 0.5 μm thick, with a bonding glass phase (Grossman, 1991; Fischer-Cripps and Lawn, 1996a; Peterson *et al.*, 1998a). Bars 3 x 4 x 25 mm are machined from as-received blocks for bonding to filled-polymer substrates.

Glass-filled polymer (Charisma, Heraeus Kulzer GmbH, Wehrheim, Germany), with properties close to those of dentin, developed for building up crowns and inlays. Charisma is a resin composite with a filler content of ≈ 60 vol% barium-alumino-borosilicate glass (mean particle size ≈ 1.5 μm) and ultrafine amorphous silica. To produce the bars, the material we squeeze from a syringe into a 3 x 4 x 25 mm Teflon mold seated on a 1.5-mm-thick glass slab with a Mylar separating strip, with a second glass slab and Mylar strip placed onto the top surface. The resulting "sandwich" is cold-pressed and light-cured (Dentacolor XS, Heraeus Kulzer GmbH, Wehrheim, Germany) for 90 sec on one side and 30 sec on the other. The cured bars are removed from the mold, and the top and bottom faces are ground flat.

Basic mechanical properties for these materials are measured as follows: Young's modulus and Poisson's ratio from a routine pulse-echo sonic technique (McSkimin, 1961; Blessing, 1988); hardness and toughness by means of Vickers indentations, hardness from measurements of impression diagonals (load/projected area of impression [Tabor, 1951], load range from 5 to 30 N), and toughness from radial crack sizes ([Anstis *et al.*, 1981], load range from 30 to 100 N).

Preparation of bilayers

Two sets of bilayer specimens were fabricated from the above components: the first to represent veneer/core all-ceramic crown structures, with a relatively low modulus material on a much stiffer substrate; and the second to simulate total-wall-thickness crowns on dentin, with a relatively hard layer on a soft substrate. The preparation protocols were as follows:

Porcelain/alumina. Alumina bars were placed in Teflon molds. Porcelain powder was mixed into a water-based slurry and applied with a paintbrush onto the substrates to a thickness ≈ 2.5 mm. After ultrasonic vibration to remove excess water from the porcelain coatings, the specimens were placed in a furnace

(Vacumat 2500 oven, Vita Zahnfabrik, Bad Sackingen, Germany) and subjected to multiple firing half-cycles with intervening cooling half-cycles in accordance with the manufacturer's specifications: (a) heat to 600°C and hold 7 min, then to 970°C and hold 1 min for sintering; (b) heat to 960°C and hold 1 min; and (c) heat to 950°C and hold 1 min. The top surfaces of the porcelain were then ground down to prescribed thicknesses, polished to 1-μm finish, and fired once more at 970°C for 1 min for glazing, followed by a final light polish.

Glass-ceramic/filled-polymer. Glass-ceramic and filled-polymer bars were diamond-polished to 1-μm finish on their prospective mating surfaces. The glass-ceramic surfaces were then etched for 60 sec (Dicor Etching Gel, Dentsply International Inc., York, PA). A sequence of bonding agents was applied to the polished surfaces: ceramic primer (3M Scotchbond, 3M Dental Products, St. Paul, MN) to the glass-ceramic surface; setting liquid (JetSet, Carl Goldberg Model Inc., Chicago, IL) to the glass-ceramic surfaces; and cyanoacrylate adhesive to the filled-polymer surfaces (Instant Jet, Carl Goldberg Model Inc., Chicago, IL). The bilayers were then brought into contact and clamped for 1.5 hr, resulting in an adhesive layer ≈ 10 μm thick. The top glass-ceramic surfaces were ground to the requisite thicknesses and polished to 1-μm finish.

Some of the bilayers were polished on their side faces, for either section-surface indentation testing or construction into "bonded-interface" specimens (Cai *et al.*, 1994b; Guiberteau *et al.*, 1994). The latter specimens were formed by the bonding of two near-identical bilayers side-face-to-side-face to form a common interface. In the case of porcelain/alumina, we achieved alignment of the specimen halves by placing the bilayers onto a common metal base plate and carefully bringing the two opposing faces together. The bilayer halves were then joined with cyanoacrylate-based adhesive (Loctite Corp., Newington, CT), clamped, and allowed to dry. For the glass-ceramic/filled-polymer, we mounted the opposing bilayer halves onto separate base plates, then clamped them together by screwing the two half-plates together along pre-aligned drilled holes, analogous to the procedure previously described for ceramic/metal bilayers (Pajares *et al.*, 1995a,b). The tops of the bonded specimens were given a final polish to ensure flat, smooth surfaces before indentation. After indentation, the specimens were separated, in the porcelain/alumina by dissolution of the adhesive in solvent and in the glass-ceramic/filled-polymer by removal of the screws.

These systems are designed to generate negligible macroscopic in-plane residual stresses during preparation, from either thermal contraction mismatch during cooling (porcelain/alumina) or from shrinkage of the adhesive during interlayer bonding (glass-ceramic/filled-polymer).

Contact damage tests

Exploratory Vickers indentations were made on the polished side surfaces of the bilayer specimens so that the integrity of the interlayer interfaces could be tested (Fig. 1A) (Wuttiphan *et al.*, 1996). These indentations were oriented so that radial cracks from the impression corners align parallel and perpendicular to the interfaces. They were centered 150 μm from the interfaces, and the loads were adjusted for each material component so that the nearest radial cracks intersected these interfaces. The indented surfaces were gold-coated for viewing in an optical microscope, by Nomarski interference illumination, and in the scanning electron microscope.

More comprehensive indentation tests were made on the bilayer specimens with Hertzian contacts used for the investigation of fundamental coating fracture modes (Fig. 1B). A tungsten carbide (WC) sphere of radius r = 3.18 mm was mounted into the crosshead of a universal testing machine (Instron 1122, Canton, MA), and the sphere driven onto the specimen top surface to peak loads up to P = 1000 N (crosshead speed 0.2 mm.min^{-1}). Bonded-interface specimens were used to reveal subsurface fracture patterns in the coatings. These specimens were mounted on a traveling micrometer stage and carefully oriented and aligned relative to the loading axis so that lines of indentations could be accurately placed along the interface

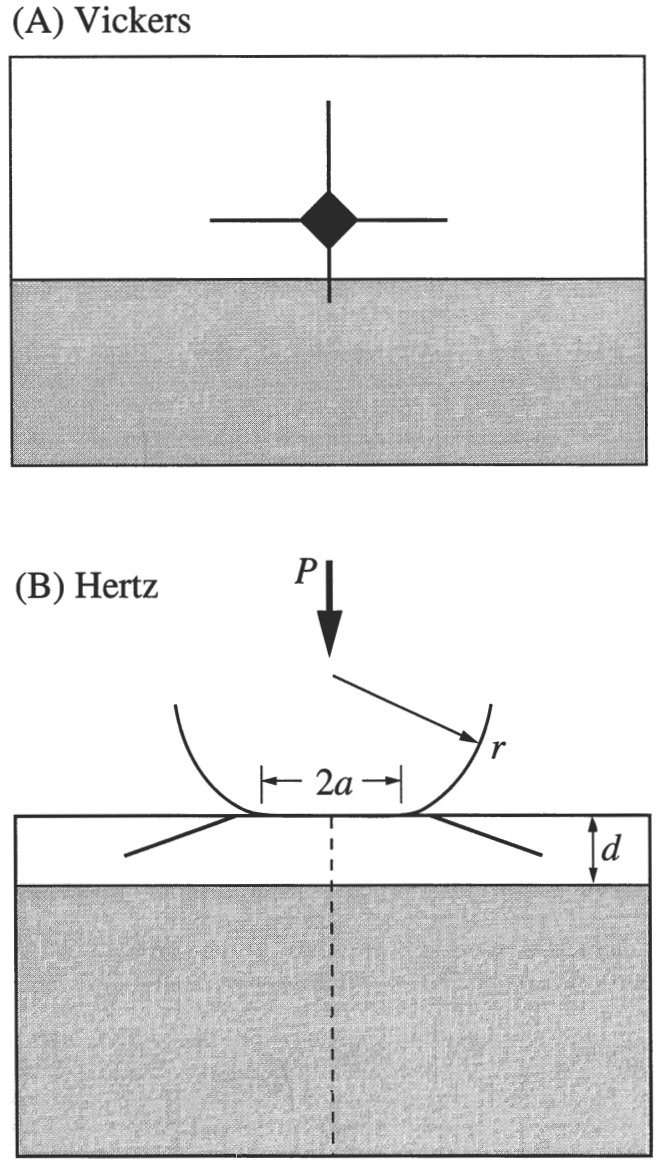

Figure 1. Schematic showing geometry for (A) Vickers indentation tests on bilayer section surfaces, and (B) Hertzian indentation tests on bilayer top surfaces.

traces (Peterson *et al.*, 1998a). After the bonded specimen halves were separated, the section surfaces were gold-coated for viewing in Nomarski interference illumination.

Critical loads for the onset of damage were measured by post-contact microscopic examination of indentation sites in the center regions of polished top surfaces (non-sectioned specimens). The indented surfaces were gold-coated for viewing in Nomarski interference contrast. An acoustic detector (LOCAN 320, Physical Acoustics Corp., Princeton, NJ) was used as an adjunct for the detection of crack initiation (Padture and Lawn, 1995; Peterson *et al.*, 1998a).

We conducted some additional Hertzian contact tests on bulk specimens of the constituent materials, using a range of sphere sizes r = 1.54 to 12.7 mm, to measure indentation stress–strain curves (Tabor, 1951; Swain and Lawn, 1969; Swain and Hagan, 1976; Guiberteau *et al.*, 1993; Cai *et al.*, 1994b) for subsequent finite element analysis. In this case, the top surfaces were gold-coated *before* indentation, so that measurements of the contact radius a could be made from impressions in the gold film as a function of load P (Guiberteau *et al.*, 1993). From these measurements, calculation of "indentation stress", $p_0 = P/\pi a^2$, and "indentation strain", a/r, facilitated construction of the indentation stress–strain curves. Measurements of the critical indentation stresses $p_0 = p_Y$ at which plastic impressions were first detected provided "yield points" on these curves.

All indentation tests were conducted in air.

Finite element modeling (FEM)

A finite element modeling (FEM) algorithm (Strand, G&D Computing Pty. Ltd., Sydney, Australia) is used for the determination of Hertzian contact stress distributions for evaluation of the fracture and deformation patterns (Fischer-Cripps and Lawn, 1996b). The algorithm models an indenting WC sphere, radius r = 3.18 mm, in frictionless axisymmetric contact at load P with an initially flat bilayer of specified coating thickness d. The contact is assumed frictionless, and the interlayer bonding is assumed infinitely strong (no delamination). The FEM grid has a minimum grid size 3 μm in the critical near-contact and interface regions—more specific details in relation to bilayer structures are given elsewhere (Pajares *et al.*, 1996a; Wuttiphan *et al.*, 1997). Contact is incremented monotonically to specified peak loads in 40 steps, with a maximum 50 iterations at each increment and with tolerance 0.1% in force and 0.5% in displacement. We can then generate stress–strain $p_0(a/r)$ functions by computing the contact radius a at each indentation load P.

The algorithm allows for the input of elastic–plastic constitutive uniaxial stress–strain responses $\sigma(\epsilon)$ for each layer material, as well as for the indenter material (Fischer-Cripps and Lawn, 1996b). Each material deforms according to a modified critical shear stress condition with linear strain hardening (Lawn and Marshall, 1998):

$$\sigma = E\epsilon, \qquad (\sigma < Y) \qquad (1a)$$

$$\sigma = Y + \alpha(\epsilon E - Y), \qquad (\sigma > Y) \qquad (1b)$$

with E Young's modulus, Y the uniaxial compression stress for the onset of yield, and α a dimensionless strain-hardening coefficient in the range $0 \leq \alpha \leq 1$ ($\alpha = 1$, fully elastic; $\alpha = 0$, fully plastic). The parameters in Eq. 1 have to be determined for each constituent material (including that of the sphere) so that computations can be made for the bilayer structures. Of these parameters, most are independently predetermined: E (and Poisson's ratio v) from the sonic technique, and Y from measurements of the critical indentation stresses $p_Y = 1.1Y$ (corresponding to the pressure at which the maximum shear stress just equals $Y/2$ (Tabor, 1951)) for initiation of plastic impressions (Fischer-Cripps and Lawn, 1996b). The only unknown is α, which we adjust to best-fit indentation stress–strain data (Fischer-Cripps and Lawn, 1996b).

Given these parameters, the FEM algorithm enables us to make point-by-point evaluation of the principal stresses below the elastic–plastic contact in the bilayers. Our primary interest lies in the tensile stresses in the coatings, for correlating with the

Table. Mechanical property parameters for constituent dental materials used in this study (means and standard deviations[a])

Material	Young's Modulus (GPa)	Poisson's Ratio	Hardness (GPa)	Yield Stress (GPa)	Work-hardening Coeff.	Toughness ($MPa.m^{1/2}$)
Porcelain (Vitadur Alpha)	63.5 ± 5	0.26 ± 0.01	6.4 ± 0.7	—	—	0.7 ± 0.1
Infiltrated alumina (InCeram)	271 ± 9	0.23 ± 0.01	12.3 ± 0.5	4.4 ± 0.4	0.40	2.9 ± 0.3
Glass-ceramic (Dicor)	69 ± 7	0.26 ± 0.01	3.8 ± 0.2	1.9 ± 0.2	0.40	1.0 ± 0.2
Filled-polymer (Charisma)	10.5 ± 2	0.41 ± 0.01	0.8 ± 0.1	0.28 ± 0.3	0.30	—
Tungsten carbide[b]	614 ± 19	0.22 ± 0.01	19.0 ± 0.5	6.0 ± 0.5	0.25	—
Enamel[c]	94 ± 5	—	3.2 ± 0.4	—	—	0.77 ± 0.05
Dentin[c]	20 ± 2	—	0.58 ± 0.05	—	—	3.1 ± 0.3[d]

[a] Standard deviations as follows: Young's modulus, single runs on 5 specimens *per* material; hardness, 15 Vickers indentations *per* specimen, 5 specimens *per* material; yield stress, 5 Hertzian indentations *per* specimen, 3 specimens *per* material; toughness, 15 Vickers indentation tests *per* specimen, 5 specimens *per* material.

[b] Data for WC from Fischer-Cripps and Lawn (1996b).

[c] Data for enamel and dentin from Xu *et al.* (1998).

[d] Data for toughness of dentin from El Mowafy and Watts (1986).

observed fracture modes. We are specifically interested in the maximum values of these tensile stresses at or just outside the contact circle on the top surface, where the cone cracks initiate, and on the contact axis at the internal coating/substrate interface, where the upward-extending cracks initiate. Of secondary interest are the shear stresses, particularly in the softer substrates where the yield condition is exceeded.

In the present computations, we neglected potential complications from any superimposed macroscopic residual stresses, and from any post-contact residual deformation field that might drive coating/substrate delamination on unloading (Fischer-Cripps and Lawn, 1996b).

Results

The Table summarizes essential material parameters for the constituent bilayer materials, including the indenter material (Fischer-Cripps and Lawn, 1996a), plus enamel and dentin (El Mowafy and Watts, 1986; Xu *et al.*, 1998) for comparison.

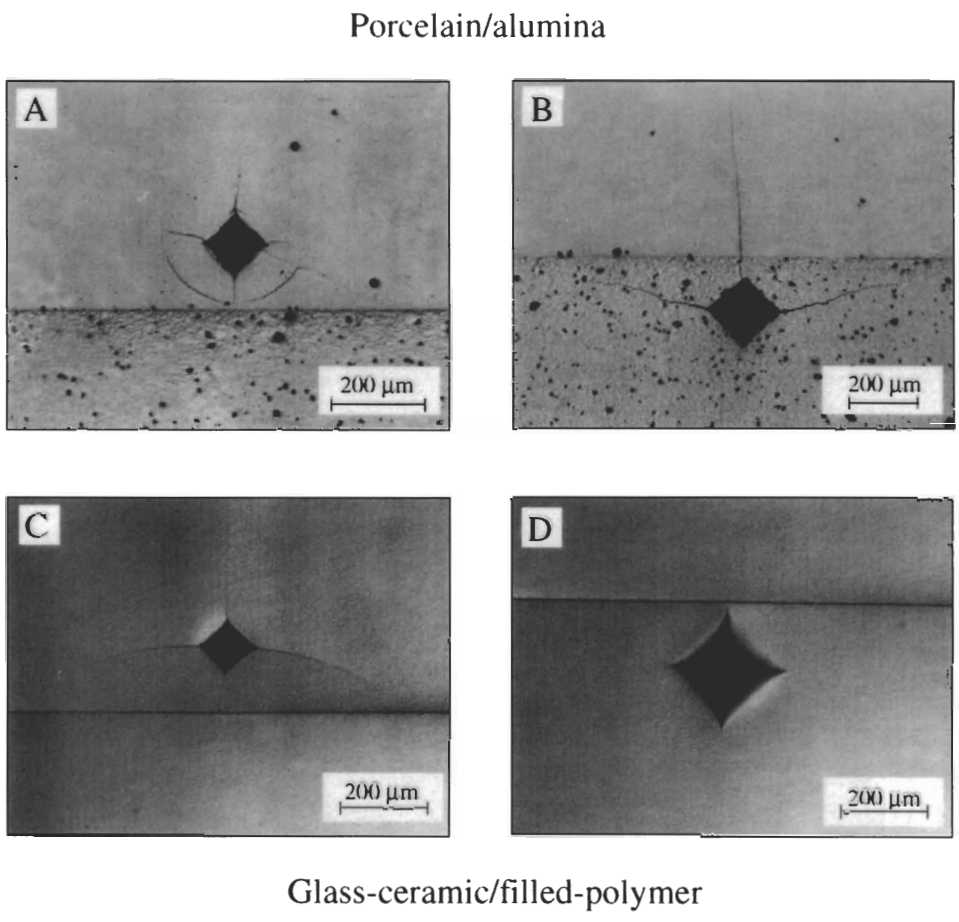

Figure 2. Vickers indentations on bilayer sections, showing behavior of radial cracks on approaching interlayer interfaces: porcelain/alumina, (A) indentation in porcelain at P = 15 N, (B) indentation in alumina at P = 50 N; glass-ceramic/filled-polymer, (C) indentation in glass-ceramic at P = 40 N, (D) indentation in filled-polymer at P = 30 N.

Vickers indentations

The results of exploratory Vickers indentations in the near-interface region on polished bilayer sections are shown for porcelain/alumina in Figs. 2A and 2B and for glass-ceramic/filled-polymer in Figs. 2C and 2D. Well-defined hardness impressions are formed, with radial cracks from the corner regions, except in the soft filled-polymer. The lower radial crack in the porcelain (Fig. 2A) does not penetrate the tougher adjacent alumina. Closer examination in the scanning electron microscope revealed no delamination of the interface, indicating strong interlayer adhesion. (Note, however, that the indentation does initiate a secondary, circumferential crack near the interface.) Conversely, the upper radial crack in the alumina (Fig. 2B) easily penetrates the less tough porcelain, although again without interfacial delamination. The sideways-extending radial cracks in this case bend toward the interface, indicating that the crack tips "sense" the presence of the adjacent, less stiff porcelain (Lardner *et al.*, 1990). In the glass-ceramic (Fig. 2C), the lower radial crack does not penetrate the adjacent layer. This time, however, scanning electron microscopy revealed extensive delamination at the interface, indicating weak interlayer adhesion. Again, the sideways radial cracks bend toward the less stiff adjoining layer. As indicated, no radial crack forms at all in the filled-polymer (Fig. 2D).

These observations reveal a variety of responses for cracks approaching interlayer interfaces, depending on the relative mechanical properties of the component materials and the interface adhesion.

Hertzian tests

Micrographs showing section views of Hertzian damage in bonded-interface specimens are shown for the two bilayer systems in Figs. 3–6, for indentations at r = 3.18 mm. These micrographs illustrate the role of contact load and coating thickness on the fracture patterns:

Porcelain/alumina. Fig. 3 shows the evolution of contact fracture in the porcelain coating as a function of load, P = 250, 500, and 1000 N, for a fixed coating thickness d = 500 μm. The visible damage consists solely of conventional cone cracks, with multiple initiations at higher loads as the expanding contact circle (AA) engulfs the first, inner ring crack on the top surface. Basically, this is the kind of crack pattern seen in porcelain monoliths. Coating failure occurs at a much higher load (P > 1900 N, not shown), at which point unrestrained

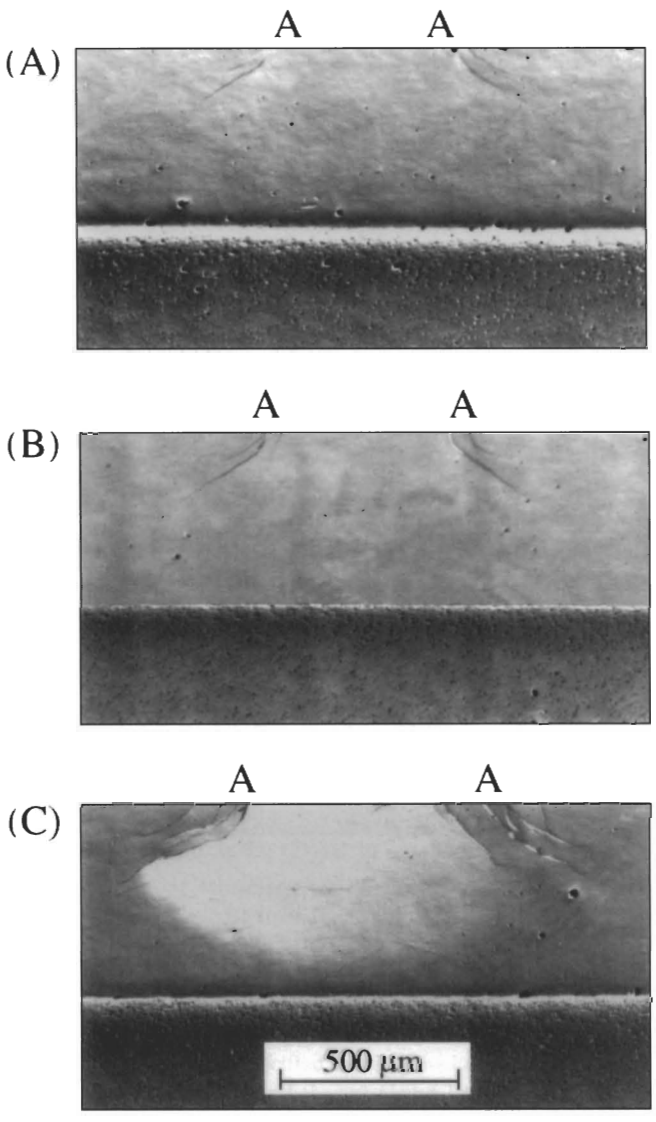

Figure 3. Damage in porcelain/alumina bilayer, from contact with WC sphere, r = 3.18 mm, coating thickness d = 500 µm, load P = (A) 250 N, (B) 500 N, (C) 1000 N. AA denotes contact diameter.

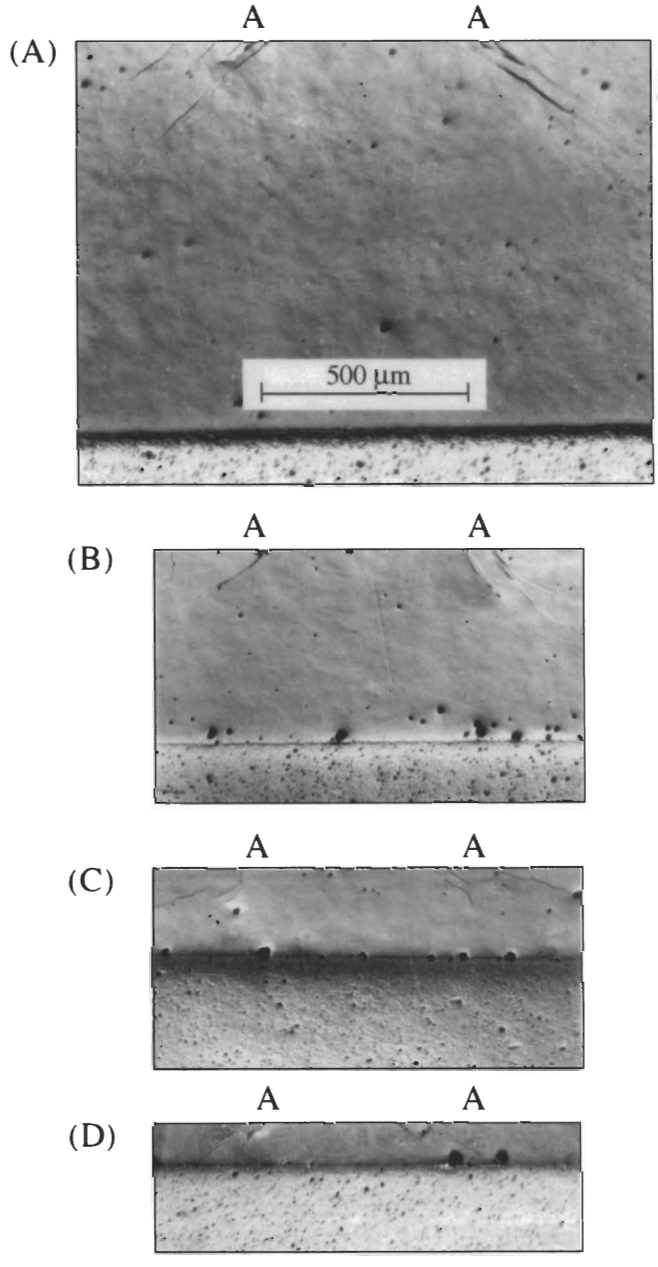

Figure 4. Damage in porcelain/alumina bilayer, from contact with WC sphere, r = 3.18 mm, load P = 500 N, coating thickness d = (A) 1000 µm, (B) 500 µm, (C) 230 µm, (D) 110 µm. AA denotes contact diameter.

crack propagation occurs through the specimen thickness, breaking the specimen into two halves. The interface reveals no sign of delamination prior to failure. Fig. 4 shows the cone crack pattern as a function of coating thickness, d = 1000, 500, 230, and 110 µm, for a fixed load P = 500 N. The cracks become shallower as d is reduced, indicating again that they "sense" the stiffer underlayer. The surface diameters of the inner ring cracks also appear to diminish slightly through the sequence in Fig. 4. When d becomes sufficiently small that the cone cracks directly intersect the interface, arrest occurs, again without delamination, implying a certain resilience in the bilayer structure.

Glass-ceramic/filled-polymer. Fig. 5 is a micrograph of the crack pattern for a glass-ceramic coating of thickness d = 1000 µm, at load P = 500 N. The crack pattern is more complex in this system, and is clearly affected by the softer underlayer. Cone-like cracks are again evident, but additional transverse cracks extending upward from the interlayer interface are also present. There are signs of incipient *quasi*-plastic deformation immediately beneath the contact in Fig. 5. Fig. 6 shows the fracture evolution as a function of load, P = 250, 500, and 750 N, in coatings of fixed thickness d = 450 µm. The crack pattern in Fig. 6A is geometrically similar to that in Fig. 5, at about half the thickness and at half the load. At the *same* load (P = 500 N) (Fig. 6B), the cracks in the thinner coating are much more proliferate, but are also highly stable—these cracks multiply rapidly, but (once initi-

ated) extend only slowly with increasing load. Note that the surface diameters of the inner surface ring cracks are much smaller in the thinner coating at this common load. Note also that, in contrast to the porcelain/alumina system, the surface ring cracks tend to occur well outside the contact circle (AA). At higher loads, somewhere between Figs. 6B and 6C (500 N < P < 750 N), the coatings fail by spalling. Some indications of *quasi*-plasticity can be discerned in the substrate, as surface rumpling, especially in Fig. 6B (although this deformation is not easily imaged in the polymer cross-sections).

In Fig. 7, the critical load P_C for crack initiation is plotted as a function of coating thickness d for the two bilayer systems, for spheres of r = 3.18 mm. Values of P_C for monolithic porcelain and glass-ceramic coating materials are included in these plots as the open boxes at the right-hand axes. For porcelain/alumina (Fig. 7A), the data exclusively represent initiation of cone cracks. Note the monotonic falloff of P_C with diminishing d, from ≈ 120 N at d = 1000 μm to ≈ 50 N at d = 50 μm. For glass-ceramic/filled-polymer (Fig. 7B), the internal upward-extending cracks initiate before the cone cracks. The value of P_C for these upward-extending cracks diminishes rapidly, from > 500 N at d = 1000 μm to < 200 N at d = 450 N.

Experimental results of indentation stress–strain tests for each of the constituent layer materials are plotted as the data points in Fig. 8. Universal curves are obtained for the monolithic materials, independent of sphere radius. The contact yield points p_Y at which plastic impressions are first observed are indicated for each material (except porcelain, for which no plasticity could be detected). Above these points, the curves exhibit some degree of nonlinearity (again, except in the porcelain). Note that in Fig. 8A the porcelain coating material is much "softer" (lower stress/strain val-

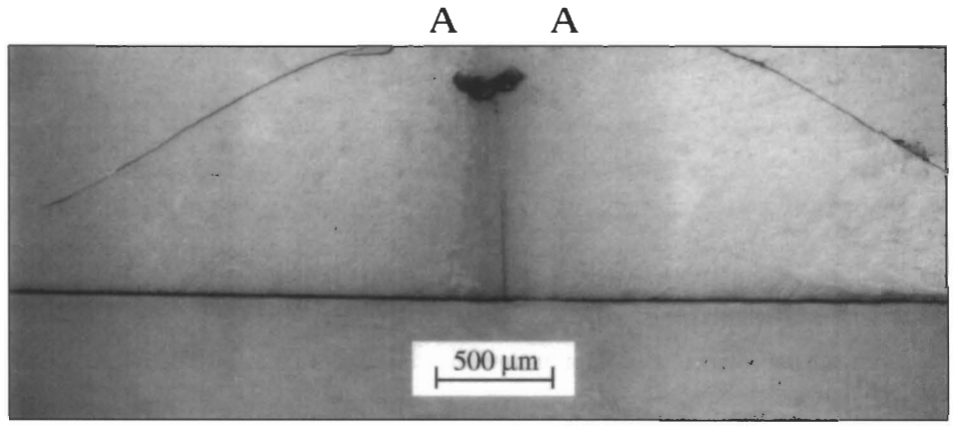

Figure 5. Damage in glass-ceramic/filled-polymer bilayer, from contact with WC sphere, r = 3.18 mm, coating thickness d = 1000 μm, load P = 500 N. AA denotes contact diameter.

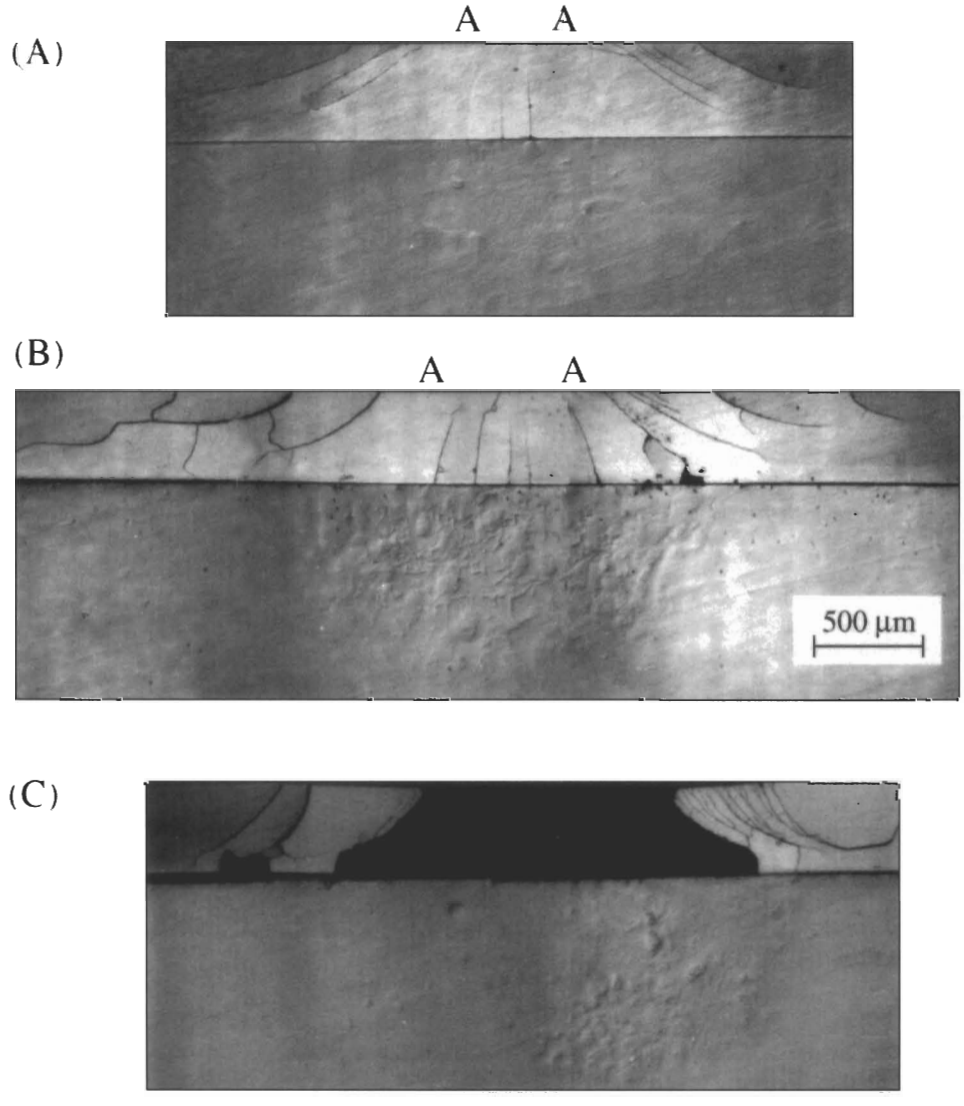

Figure 6. Damage in glass-ceramic/filled-polymer bilayer, from contact with WC sphere, r = 3.18 mm, coating thickness d = 450 μm, load P = (A) 250 N, (B) 500 N, (C) 750 N. AA denotes contact diameter.

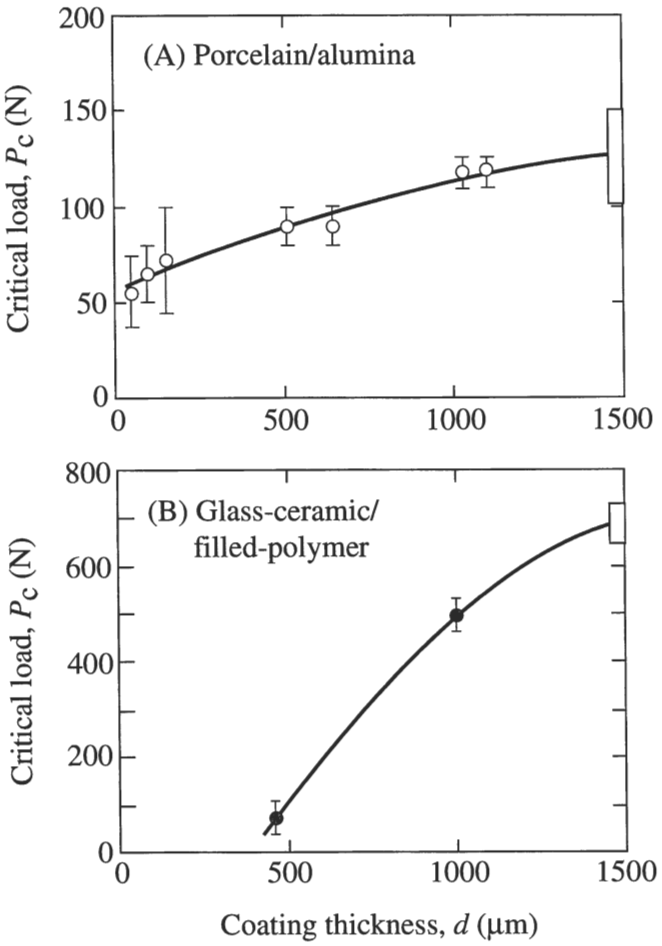

Figure 7. Critical load for fracture in bilayer as function of coating thickness: (A) porcelain/alumina, initiation of cone cracks; (B) glass-ceramic/filled-polymer, initiation of upward-extending transverse cracks. Boxes at right axes denote critical loads for cone cracks in coating monoliths. Indentations made at crosshead speed 0.2 mm.min^{-1}. Data points represent means and standard deviations, 5 indentations per point.

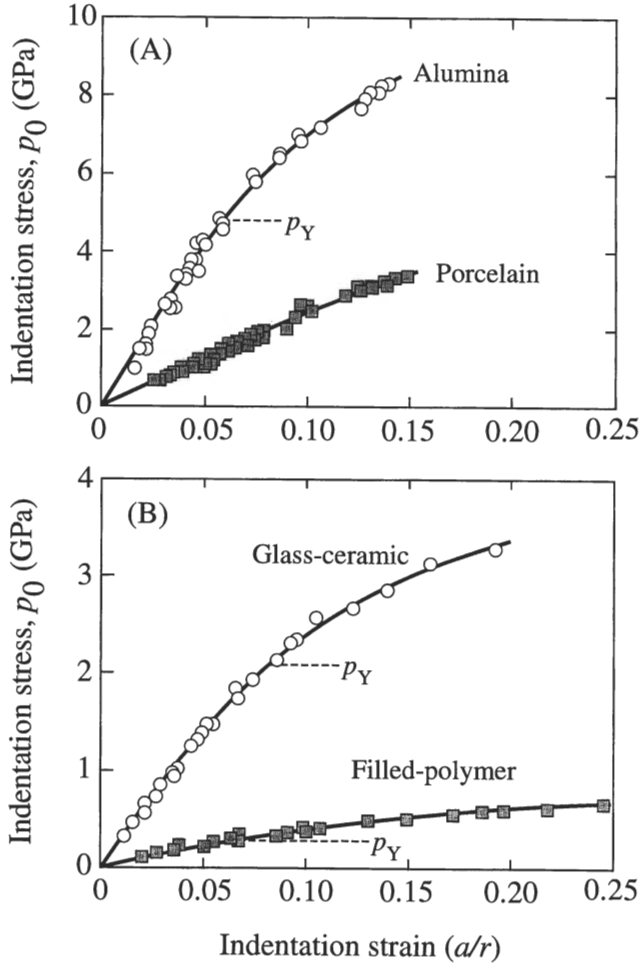

Figure 8. Indentation stress–strain curves for materials used in bilayer systems: (A) porcelain and alumina; (B) glass-ceramic and filled-polymer. Data points are experimental results; solid curves are FEM fits. Values of contact stress p_Y at first yield indicated. Sphere radii r = 1.54–12.7 mm (not distinguished in plots). Data points represent individual indentations made on 3 polished specimens of each material at a crosshead speed 0.2 mm.min^{-1}.

ues) than the alumina substrate; conversely, in Fig. 8B the glass-ceramic coating is much "harder" than the filled-polymer substrate. These trends are consistent with the relative modulus and hardness values in the Table.

Stress analysis (FEM)

We "calibrated" the FEM algorithm by adjusting α in Eq. 1 to best-fit the stress–strain data for the monolithic materials in the nonlinear regions of Fig. 8. Regenerated FEM curves based on the parameters from the Table are shown as the solid curves in Fig. 8.

Fig. 9 shows FEM-generated contours of principal tensile stress in the porcelain/alumina bilayer, d = 500 μm, and the glass-ceramic/filled-polymer bilayer, d = 450 μm, for Hertzian contacts with WC sphere, r = 3.18 mm, at P = 500 N (corresponding to the contact conditions in Figs. 3B and 6B). In the porcelain/alumina (Fig. 9A), the maximum tensile stress contours (shaded) are highly concentrated at the top surface immediately outside the contact circle. Note the inverted mushroom-shaped compression zone (unshaded) extending outward below the surface tensile zone. In the glass-ceramic/filled-polymer (Fig. 9B), the location of the maximum tensile stress contours shifts to the interlayer interface below the contact. However, the tensile stresses remain high on the top surface, although the contours spread out much farther from the contact circle. In this system, the intense tensile stresses at the internal interface indicate flexure of a stiff coating on a relatively soft substrate. Note the spatial correlations between the tensile stress maxima in Fig. 9 and the cracks in the two bilayer systems in Figs. 3–6.

Also shown in Fig. 9B is the FEM-generated yield-zone contour (dashed curve) in the polymer substrate. This contour correlates with the damage zone noted in the corresponding bonded-interface section (Fig. 6B). No such yield zone was predicted in the porcelain/alumina bilayers over the load range studied.

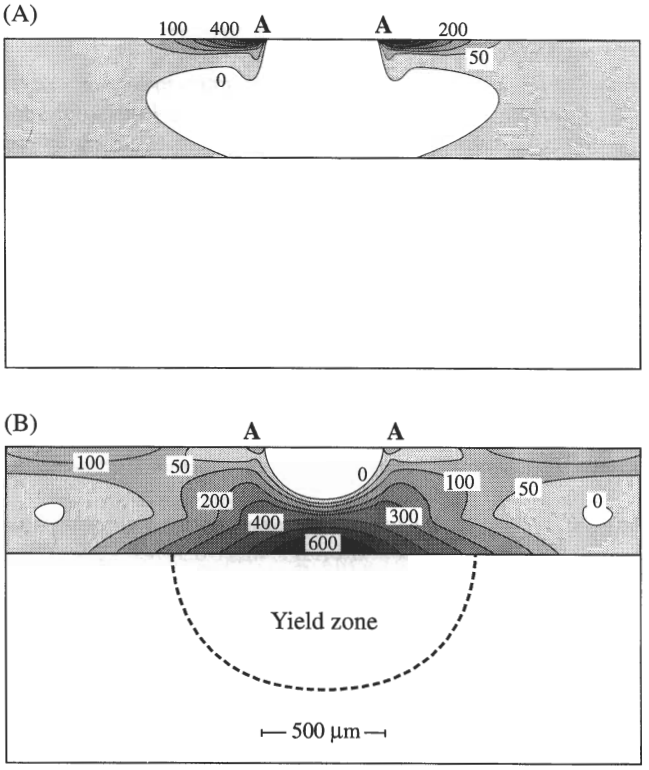

Figure 9. FEM-generated stress contours from contact with WC sphere, $r = 3.18$ mm, $P = 500$ N: (A) porcelain/alumina bilayer, $d = 500$ μm; (B) glass-ceramic/filled-polymer bilayer, d = 450 _m. Contours in coating, principal tensile stresses (MPa). Dashed curve in substrate in (B) is predicted yield zone. AA denotes contact diameter.

Discussion

Our study on contact damage in model bilayers with WC spheres ($r = 3.18$ mm) reveal widely different modes of coating fracture, critically dependent on relative elastic–plastic properties as well as on coating thickness:

Porcelain/alumina (soft coating/hard substrate). At a critical contact load, classic cone cracks form in the porcelain, in the thicker coatings indistinguishable from those in monolithic specimens (Peterson *et al.*, 1998a). These cone cracks propagate with increasing load (Fig. 3), until the expanding contact circle engulfs the surface ring traces (Peterson *et al.*, 1998a). Multiple surface rings then form, but no other crack system can be observed in the coating. As the coatings are made thinner, the cone crack depths become progressively smaller (Fig. 4), as if "repelled" by the underlying substrate. The appearance of a compression zone in the FEM-generated stress contours (Figs. 3 and 4) accounts for this reluctance of the cone cracks to approach the porcelain/alumina interface. Such inhibition is expected behavior for cracks approaching stiff adjoining layers (Fett and Munz, 1997). Even in the thinnest coatings, where the cracks finally penetrate the interface into the tougher substrate (Table), the bilayer structures remain intact, without delamination (Fig. 4D). Ultimately, at very high loads, failure occurs by crack propagation through the entire bilayer. It is instructive to note the large range between the loads for first initiation of the cone cracks ($P_C \approx 90$ N at $d = 500$ μm, Fig. 7A) and ultimate bilayer failure ($P > 1900$ N at $d = 500$ μm), indicative of a highly damage-tolerant structure.

Glass-ceramic/filled-polymer (hard coating/soft substrate). In this system, both cone cracks and upward-extending cracks propagate in the glass-ceramic coatings (Fig. 5). For the coating thicknesses studied here ($d \leq 1$ mm), the latter cracks initiate first, from the internal interface. (Independent experiments on analogous bilayer systems using serial polishing from the top indented surface demonstrated that these cracks initiate as inverted axisymmetric cones, but subsequently branch outward from the contact axis in radial fashion at high loads [Wuttiphan, 1997].) With increasing load, both crack types extend transversely across the coating in a highly stabilized manner (Fig. 6). The crack stability is attributed to the "flexural" stressing in the plate-like coating on a soft supporting underlayer (Lee *et al.*, 1998). The strong stress gradients across the coating section (Fig. 9B) are consistent with the deflection and stabilization of cracks observed in the glass-ceramic coatings (Figs. 5 and 6). This stabilization, combined with the lateral spreading of the tensile stress contours in Fig. 9B, explains the observed multiplicity of cracks in this bilayer system. Ultimately, failure occurs by catastrophic propagation of one or other such transverse cracks through the coating at high load, followed by spalling at the relatively weak, delaminated interface. Again, it is instructive to note the wide range of loads between crack initiation ($P_C \approx 150$ N at $d = 450$ μm, Fig. 7B) and failure ($P > 700$ N at $d = 450$ μm, Fig. 6C). Hence, both bilayer systems offer some form of damage tolerance, even though the fracture modes are quite different.

The coating fracture patterns observed in the two bilayer systems correlate with the locations of maximum tensile stresses evaluated from finite element modeling of the Hertzian contact. In the porcelain/alumina (Fig. 9A), the maximum tensile stresses occur at the top surface, where cone cracks initiate, and are compressive at the internal interface, where the cracks ultimately intersect. In the glass-ceramic/filled-polymer (Fig. 9B), the interior interface tensile stresses are dominant, although the surface stresses are still positive, consistent with the appearance of two crack modes in the coating. Such correlations have been previously described in relation to elastic mismatch (Anusavice and Tsai, 1997).

The FEM analysis described here allows for both elastic and plastic mismatch in the layer materials (*via* the nonlinear indentation stress–strain curves in Fig. 8). Elastic mismatch alone may not always be sufficient to account for the crack patterns in bilayer structures. Transverse cracks have been observed to form at internal interfaces in glass/glass-ceramic bilayers designed with *zero* mismatch in elastic modulus, but with low relative yield stress in the glass-ceramic substrate (Wuttiphan *et al.*, 1996). In this context, yield zones of the kind observed in the polymer substrate (Fig. 6B) and predicted by the FEM calculations (Fig. 9B) may well enhance the tensile stresses that drive the coating fractures.

It is of interest to consider the above results in relation to

clinical failures of ceramic crowns (Scherrer and de Rijk, 1993; Scherrer *et al.*, 1994; Kelly, 1997). As intimated in the "Introduction", ceramic restorations ideally have outer thicknesses > 1 mm, but may be much thinner near the margins. Masticatory forces on molar teeth can exceed 200 N (DeLong and Douglas, 1983; Anusavice, 1989; Phillips, 1991; Craig, 1997), with forces up to 800 N in extreme conditions (e.g., bruxing) (Kelly, 1997), and the characteristic cuspal radii of opposing teeth typically lie within the 2– to 4-mm range (Wheeler, 1958). Our choices of bilayer thicknesses and Hertzian test variables embrace these broad ranges. The implications from our single-cycle studies in air are that current bilayer structures require loads above the upper end of the oral range to bring about catastrophic failure. While this suggests remarkably resilient structures, it must be remembered that cracks can initiate at relatively low contact loads, in both porcelain and glass-ceramic materials; glass-ceramics are also susceptible to *quasi*-plastic damage (Cai *et al.*, 1994a,b). Both fracture and *quasi*-plastic damage (particularly the latter) also tend to intensify with repetitive loading ("cyclic fatigue" [Guiberteau *et al.*, 1993; Cai *et al.*, 1994a; Padture and Lawn, 1995]), and with increasing water content in the environment (Guiberteau *et al.*, 1993). This raises the prospect of damage accumulation in such materials under sustained chewing, even at moderate loads (White *et al.*, 1995, 1997). For potential oral lifetimes to be quantified, contact fatigue studies, in water as well as in air, coupled with measurements of bilayer strengths after contact damage accumulation (Peterson *et al.*, 1998a), need to be performed.

Acknowledgments

V.P. Thompson, S. Likitvanichkul, and J.M. Antonucci provided valuable assistance with the preparation of the glass-ceramic/filled-polymer bilayer specimens, and E.E. Parry with the porcelain/alumina. J. Cline performed the x-ray analysis of the porcelain. G.V. Blessing and J.A. Slotwinski assisted in obtaining the elastic modulus values. We thank V.P. Thompson, J.R. Kelly, and A.C. Fischer-Cripps for helpful discussions on various aspects of this work. The generous supply of materials from K. Chyung at Corning Inc., H. Hornberger at Vita Zahnfabrik, and Heraeus Kulzer is acknowledged. This work was partially funded under NIDR Grant PO1 DE10976, and internally by NIST. Y.-G.J. acknowledges financial support from the Korea Science and Engineering Foundation, and S.W. from a Royal Thai Scholarship.

References

An L, Chan HM, Padture NP, Lawn BR (1996). Damage-resistant alumina-based layer composites. *J Mater Res* 11:204-210.

Anstis GR, Chantikul P, Marshall DB, Lawn BR (1981). A critical evaluation of indentation techniques for measuring fracture toughness: I. direct crack measurements. *J Am Ceram Soc* 64:533-538.

Anusavice KJ (1989). Criteria for selection of restorative materials: properties vs technique sensitivity. In: Quality evaluations of dental restorations. Anusavice KJ, editor. Chicago: Quintessence, pp. 15-56.

Anusavice KJ, Tsai YL (1997). Stress distribution in ceramic crown forms as a function of thickness, elastic modulus, and supporting substrate. In: Proceedings of the sixteenth Southern Biomedical Engineering Conference. Bumgardner JD, Puckett AD, editors. Biloxi, MS, pp. 264-267.

Blessing GV (1988). The pulsed ultrasonic velocity method for determining material dynamic elastic moduli. In: Symposium on dynamic modulus measurements. Wolfenden A, editor. Kansas City, MO: ASTM, pp. 47-57.

Cai H, Kalceff MAS, Hooks BM, Lawn BR, Chyung K (1994a). Cyclic fatigue of a mica-containing glass–ceramic at Hertzian contacts. *J Mater Res* 9:2654-2661.

Cai H, Stevens Kalceff MA, Lawn BR (1994b). Deformation and fracture of mica-containing glass–ceramics in Hertzian contacts. *J Mater Res* 9:762-770.

Claus H (1990). Vita InCeram, a new system for producing aluminum oxide crown and bridge substructures. *Quintessenz Zahntech* 16:35-46.

Craig RG (1997). Mechanical properties. In: Restorative dental materials. Craig RG, editor. St. Louis: Mosby, Chapter 4.

DeLong R, Douglas WH (1983). Development of an artificial oral environment for the testing of dental restoratives: bi-axial force and movement control. *J Dent Res* 62:32-36.

El Mowafy OM, Watts DC (1986). Fracture toughness of human dentin. *J Dent Res* 65:677-681.

Fett T, Munz D (1997). Stress intensity factors and weight functions. Southampton, UK: Computational Mechanics Publications, Ch. 13.

Fischer-Cripps AC, Lawn BR (1996a). Indentation stress–strain curves for "*quasi*-ductile" ceramics. *Acta Metallurgica et Materiala* 44:519-527.

Fischer-Cripps AC, Lawn BR (1996b). Stress analysis of contact deformation in *quasi*-plastic ceramics. *J Am Ceram Soc* 79:2609-2618.

Giordano RA (1996). Dental ceramic restorative systems. *Compendium* 17:779-794.

Grossman DG (1991). Structure and physical properties of Dicor/MGC glass-ceramic. In: Proceedings of the International Symposium on Computer Restorations. Mörmann WH, editor. Chicago, IL: Quintessence Publishing Co., pp. 103-115.

Guiberteau F, Padture NP, Cai H, Lawn BR (1993). Indentation fatigue: a simple cyclic Hertzian test for measuring damage accumulation in polycrystalline ceramics. *Philos Mag* 68(A):1003-1016.

Guiberteau F, Padture NP, Lawn BR (1994). Effect of grain size on Hertzian contact in alumina. *J Am Ceram Soc* 77:1825-1831.

Hornberger H, Marquis PM, Christiansen S, Strunk HP (1996). Microstructure of a high strength alumina glass composite. *J Mater Res* 11:855-858.

Kelly JR (1997). Ceramics in restorative and prosthetic dentistry. *Ann Rev Mater Sci* 27:443-468.

Lardner TJ, Ritter JE, Shiao ML, Lin MR (1990). Behavior of indentation cracks near free surfaces and interfaces. *Int J Fract* 44:133-143.

Lawn BR, Marshall DB (1998). Nonlinear stress–strain curves for solids containing closed cracks with friction. *J Mech Phys Solids* 46:85-113.

Lawn BR, Padture NP, Cai H, Guiberteau F (1994). Making ceramics "ductile". *Science* 263:1114-1116.

Lawn BR, Lee SK, Peterson IM, Wuttiphan S (1998). A model of strength degradation from Hertzian contact damage in tough ceramics. *J Am Ceram Soc* 81:1509-1520.

Lee KS, Wuttiphan S, Hu XZ, Lee SK, Lawn BR (1998). Contact-induced transverse fractures in brittle layers on soft substrates: a study on silicon nitride bilayers. *J Am Ceram Soc* 81:571-580.

Lee KS, Lee SK, Lawn BR, Kim DK. Contact damage and strength degradation in brittle/*quasi*-plastic silicon nitride bilayers. *J Am Ceram Soc* (in press).

McSkimin HJ (1961). Pulse-superposition methods for measuring ulatrasonic wave velocities in solids. *J Acoust Soc Am* 33:12-16.

Mulhearn TO (1959). The deformation of metals by Vickers-type pyramidal indenters. *J Mech Phys Solids* 7:85-96.

Padture NP, Lawn BR (1995). Contact fatigue of a silicon carbide with a heterogeneous grain structure. *J Am Ceram Soc* 78:1431-1438.

Pajares A, Guiberteau F, Lawn BR (1995a). Hertzian contact damage in magnesia-partially-stabilized zirconia. *J Am Ceram Soc* 78:1083-1086.

Pajares A, Wei L, Lawn BR (1995b). Damage accumulation and cyclic fatigue in Mg-PSZ at Hertzian contacts. *J Mater Res* 10:2613-2625.

Pajares A, Wei LH, Lawn BR, Berndt CC (1996a). Contact damage in plasma-sprayed alumina-based coatings. *J Am Ceram Soc* 79:1907-1914.

Pajares A, Wei LH, Lawn BR, Padture NP, Berndt CC (1996b). Mechanical characterization of plasma-sprayed ceramic coatings on metal substrates by contact testing. *Mater Sci Eng* 208(A):158-165.

Peterson IM, Pajares A, Lawn BR, Thompson VP, Rekow ED (1998a). Mechanical characterization of dental ceramics using Hertzian contacts. *J Dent Res* 77:589-602.

Peterson IM, Wuttiphan S, Pajares A, Lawn BR (1998b). Role of microstructure on contact damage and strength degradation of micaceous glass-ceramics. *Dent Mater* 14:80-89.

Phillips RW (1991). Skinner's science of dental materials. Philadelphia: W.B. Saunders.

Probster L (1993). Survival rate of In-Ceram restorations. *Int J Prosthodont* 6:259-263.

Probster L, Diehl J (1992). Slip casting alumina ceramics for crown and bridge restorations. *Quintessence Dent Technol* 23:25-31.

Rinke S, Huls A, Jahn L (1995). Marginal accuracy and fracture strength of conventional and copy-milled all-ceramic crowns. *Int J Prosthodont* 8:303-310.

Scherrer SS, de Rijk WG (1993). The fracture resistance of all-ceramic crowns on supporting structures with different elastic moduli. *Int J Prosthodont* 6:462-467.

Scherrer SS, de Rijk WG, Belser UC, Meyer J-M (1994). Effect of cement film thickness on the fracture resistance of a machinable glass-ceramic. *Dent Mater* 10:172-177.

Swain MV, Hagan JT (1976). Indentation plasticity and the ensuing fracture of glass. *J Phys D: Appl Phys* 9:2201-2214.

Swain MV, Lawn BR (1969). A study of dislocation arrays at spherical indentations in LiF as a function of indentation stress and strain. *Phys Stat Sol* 35:909-923.

Tabor D (1951). Hardness of metals. Oxford: Clarendon.

Wheeler RC (1958). A textbook of dental anatomy and physiology. Philadelphia, PA: W.B. Saunders.

White SN, Zhao XY, Zhaokun Y, Li ZC (1995). Cyclic mechanical fatigue of a feldspathic dental porcelain. *Int J Prosthodont* 8:413-420.

White SN, Li ZC, Yu Z, Kipnis V (1997). Relationship between static chemical and cyclic mechanical fatigue in a feldspathic porcelain. *Dent Mater* 13:103-110.

Wolf WD (1995). Strength and fracture toughness of alumina-glass dental composites prepared by melt-infiltration (PhD dissertation). University of Minnesota.

Wolf WD, Vaidya KJ, Francis LF (1996). Mechanical properties and failure analysis of alumina-glass dental composites. *J Am Ceram Soc* 79:1769-1776.

Wuttiphan S (1997). Contact damage and fracture of ceramic layer structures (PhD dissertation). University of Maryland.

Wuttiphan S, Lawn BR, Padture NP (1996). Crack suppression in strongly-bonded homogeneous/heterogeneous laminates: a study on glass/glass-ceramic bilayers. *J Am Ceram Soc* 79:634-640.

Wuttiphan S, Pajares A, Lawn BR, Berndt CC (1997). Effect of substrate and bond coat on contact damage in zirconia-based plasma coatings. *Thin Solid Films* 293:251-260.

Xu HHK, Smith DT, Jahanmir S, Romberg E, Kelly JR, Thompson VP, *et al.* (1998). Indentation damage and mechanical properties of human enamel and dentin. *J Dent Res* 77:472-480.